Title
Excited State Absorption and Fluorescence Line Narrowing Studies of Cm{sub 3+} in LuPO{sub 4}

Journal
Journal of Chemical Physics, 105(7)

Author
Murdoch, K.M.

Publication Date
1996

LBL-38503
UC-401
Preprint

Lawrence Berkeley Laboratory
UNIVERSITY OF CALIFORNIA

CHEMICAL SCIENCES DIVISION

Submitted to Journal of Chemical Physics

Excited State Absorption and Fluorescence Line Narrowing Studies of Cm^{3+} in $LuPO_4$

K.M. Murdoch, N.M. Edelstein, L.A. Boatner, and M.M. Abraham

January 1996

Prepared for the U.S. Department of Energy under Contract Number DE-AC03-76SF00098

DISCLAIMER

LBL-38503
UC-401

Excited State Absorption and Fluorescence Line Narrowing Studies of Cm^{3+} in $LuPO_4$

K.M. Murdoch,* N.M. Edelstein,* L.A. Boatner,** and M.M. Abraham**

*Chemical Sciences Division, Ernest Orlando Lawrence Berkeley National Laboratory, University of California, Berkeley, CA 94720
**Solid State Division, Oak Ridge National Laboratory, Oak Ridge, TN 37831

January 1996

This work was supported by the Director, Office of Energy Research, Office of Basic Energy Sciences, Chemical Sciences Division, of the U.S. Department of Energy under Contract No. DE-AC03-76SF00098, and by the Division of Material Sciences, U.S. Department of Energy under Contract No. DE-AC05-84OR21400 with Martin Marietta Energy Systems, Inc.

Excited State Absorption and Fluorescence Line Narrowing Studies of Cm^{3+} in $LuPO_4$

K. M. Murdoch and N. M. Edelstein

Chemical Sciences Division, Lawrence Berkeley National Laboratory,

Berkeley, CA 94720, USA

L. A. Boatner and M. M. Abraham

Solid State Division, Oak Ridge National Laboratory,

Oak Ridge, TN 37831, U.S.A

Abstract

Laser selective excitation, fluorescence line narrowing, and excited state absorption techniques have been used to investigate the electronic-energy-level stucture of the $5f^7$ ion Cm^{3+} in the host crystal $LuPO_4$. Crystal-field levels have been determined up to 35,700 cm^{-1} for the principal D_{2d} symmetry site. Eighty levels have been assigned and fitted to a parametric Hamiltonian with an rms deviation of 28.4 cm^{-1}. Inhomogeneous broadening of the electronic transitions and the small 9.5 cm^{-1} splitting of the nominally $^8S_{7/2}$ ground multiplet are responsible for satellite lines reported previously. Time resolved fluorescence line narrowing was used to observe energy transfer between different subsites of the intinsic Cm^{3+} center. It was found that electric-dipole interactions mediate this energy transfer.

Introduction

The ground configuration of the actinide ion Cm^{3+} is a half-filled shell comprised of the Rn core and seven 5f electrons ($5f^7$). In the limit of pure Russell-Saunders coupling the ground electronic state will be ^8S. However, for a heavy ion such as Cm^{3+} (atomic number Z = 96) spin-orbit coupling effects are large and the resulting intermediate-coupled wavefunction is only about 79% $^8S_{7/2}$. For a pure S state ion the crystal-field splitting should be identically zero. In Cm^{3+} complexes the splitting of the ground $J = {}^7/_2$ term is on the order of 2 - 50 cm^{-1}. For other half-filled shell configurations such as Gd^{3+} (Xe core and $4f^7$) and the d^5 transition metal ions, the ground term crystal-field splitting is less than 1 cm^{-1}. [1-3]

Recently, a number of reports [4,5] have been published on the electron paramagnetic resonance (EPR) and optical spectra of Cm^{3+} ions diluted in a single crystal of $LuPO_4$. The Cm^{3+} ion substitutionally replaces a Lu^{3+} ion at the D_{2d} symmetry site. The ground $J = {}^7/_2$ multiplet consists of four Kramers' doublets with a total splitting of 9.5 cm^{-1}. In these earlier studies $Cm^{3+}/LuPO_4$ crystal-field levels up to 34,000 cm^{-1} were measured primarily by absorption spectroscopy and fitted to the parameters of an empirical Hamiltonian. Two-photon absorption has also been observed to three of the Cm^{3+} multiplets and the polarization behavior of these transitions analyzed using second- and third-order theory [6]. All of these levels belong to the intrinsic Cm^{3+} center. Two minor Cm^{3+} sites were also distinguished by laser-selective-excitation (LSE) spectroscopy [5].

In this study, LSE spectroscopy was used to obtain additional experimental energy levels of the intrinsic center. Its absorption transitions were found to exhibit inhomogeneously-broadened FWHM line widths of at least 2.3 cm^{-1}. This compares to an overall crystal-field splitting of the nominally $^8S_{7/2}$ ground state of 9.5 cm^{-1} [5], with all

four ground-state levels thermally populated at 4.2 K. Fluorescence line narrowing (FLN) has been used to resolve these ground-state splittings. In FLN experiments the observed line widths are limited by the either the bandwidth of the laser line or the resolution of the monochrometer, so the energies of many of the levels found previously by absorption spectroscopy could be determined more accurately.

Many excited levels also exhibit lifetime broadening due to the quenching effect of multi-phonon decay processes. Multi-phonon decay is most efficient in regions containing many close lying crystal-field levels. For the Cm^{3+} ion there are dense regions of levels between 24,500 and 26,500 cm^{-1}, and above 29,000 cm^{-1}. Such non-radiative decay processes broaden the observed absorption transitions, which makes it difficult to resolve the ground-state splittings and so determine precisely the energy of each excited level. It is also difficult to distinguish contributions to the observed transition from each of the four ground-state crystal-field levels in polarization experiments.

A sequential excitation scheme using the output of two dye lasers allowed the observation of excitation transitions originating from the isolated-metastable $^6P_{7/2}$ level at 16,528 cm^{-1}. This level had a measured lifetime of (580±60) μs and a Γ_7 D_{2d} symmetry assignment [5]. Although the line widths for excited-state absorption (ESA) were similar to those for ground-state absorption (GSA), just one transition was observed to each excited level. By using this technique levels were accessible up to 40,600 cm^{-1}. A similar method was used by Stump *et al.* [7] to observe anti-Stokes luminescence from the Cm^{3+} trihalides.

Inter-ion energy transfer can be observed by time resolved fluorescence line narrowing (TRFLN) [8]. In this case energy is transferred between different intrinsic

Cm^{3+} subsites within the inhomogeneously-broadened GSA transitions. This is believed to be the first example of inter-ion energy transfer involving Cm^{3+} ions.

As mentioned earlier, for Cm^{3+} ions there is significant mixing of the L-S states due to strong spin-orbit coupling. To avoid ambiguity in the labeling of the multiplets, $^6D_{7/2}$ will be used to denote the multiplet at 16,800 cm^{-1}, while $^6D_{7/2}{}'$ (distinguished by a prime) will be used for the multiplet at 27,900 cm^{-1}. The nomenclature $^{2S+1}L_J(n)$ will be used to indicate the n^{th} highest energy level in the multiplet $^{2S+1}L_J$.

Experimental

A single crystal of $LuPO_4$ doped with almost isotopically pure ^{248}Cm was grown using the high-temperature solution technique described previously [9,10]. It was relatively small, with dimensions of 0.5 x 1.0 x 2.0 mm^3. The nominal Cm^{3+} concentration is estimated to be less than 0.1 mole%. This radioactive sample was sealed in a quartz ampoule for containment purposes under a partial pressure of helium.

All the experiments, unless otherwise stated, were conducted with the sample cooled to 4.2 K using an Oxford Instruments model CF1204 optical cryostat. Thermal conduction between the sample and the heat exchanger was by means of a helium exchange gas. Heating coils and an Oxford Instruments model ITCV4 temperature controller were sometimes used to raise the sample temperature. A rhodium-iron temperature sensor was attached to the outside of the inner chamber which contained the sample.

GSA spectra were obtained using a Spectra Physics model PDL-3 dye laser pumped by the second- or third-harmonic output of a Spectra Physics model GCR-3

Nd:YAG laser. A number of dyes were used to cover the spectral range from 16,400 to 26,300 cm^{-1}. These are listed in Table 1. The $^6D_{7/2}(1) \rightarrow {}^8S_{7/2}(1)$ fluorescence, centered at 16,528 cm^{-1}, was analyzed using a Spex model 1403 double monochrometer and detected by a thermoelectrically cooled Hamamatsu R375 photo-multiplier tube. The slit widths were always less than 100 μm in order to achieve FLN and were set according to the strength of the absorption transitions. Neutral density filters were sometimes used to avoid pulse pile up. The signal was amplified by a Stanford Research model SR445 fast preamplifier and measured using a Stanford Research model SR400 gated photon counter. The $^6D_{7/2}$ fluorescence lifetime is 580 μs and time-gate widths of between 150 and 400 μs were used. Ground state absorption spectra were recorded for the study reported previously [5], using a Xe lamp and the Spex monochrometer.

ESA spectra were obtained using two Spectra Physics pulsed dye lasers. The first pulse was produced by a model PDL-1 dye laser pumped by the second-harmonic output of a DCR-1 Nd:YAG laser. Rhodamine 640 dye was used to pump the $^8S_{7/2}(1) \rightarrow {}^6D_{7/2}(1)$ transition and so populate the $^6D_{7/2}$ multiplet. The second pulse, after a delay time of approximately 10 μs, was produced by the PDL-3 dye laser using one of the dyes listed in Table 1. The two pump lasers and the detection electronics were triggered externally using a Systron Donner model 100A pulse generator. Both laser beams were steered with mirrors onto the main focusing lens. They were focused to the same spot in the crystal using a 25 cm quartz lens. The polarization of the first beam was always parallel to the crystallographic c-axis. An Optics for Research Model SB-10 Soleil-Babinet compensator was used to rotate the polarization of the second beam for polarization experiments.

Fluorescence from the $^6P_{5/2}$ multiplet, centered at 19,777 cm^{-1}, was analyzed and detected. A slit width of 400 μm was used to ensure throughput of most of the $^6P_{5/2} \rightarrow {}^8S_{7/2}$ fluorescence. The signal was then amplified and measured with a Stanford Research

model SR250 gated integrator and boxcar averager. The $^6P_{5/2}$ fluorescence lifetime is approximately 100 ns due to fast non-radiative relaxation to the $^6D_{7/2}$ multiplet, so a small gate width of 200ns was used. Site selectivity within the inhomogeneously-broadened transitions was possible due to the 0.8 cm^{-1} line width of the PDL-1 dye laser. Only the subset of sites excited by the first laser pulse contributed to the observed ESA.

Theoretical

The observed energy levels were fitted to a phenomenological Hamiltonian $H = H_{FI} + H_{CF}$ by a simultaneous diagonalization of the free-ion Hamiltonian H_{FI} and the crystal-field Hamiltonian H_{CF}. The free-ion Hamiltonian is given by the expression [1,11]:

$$H_{FI} = \sum_{k=0,2,4,6} F^k(nf,nf) f_k + \zeta_f \alpha_{S.O.} + \alpha L(L+1) + \beta G(G_2) + \gamma(R_7) + \sum_{\substack{k=2,8 \\ k \neq 5}} T^k t_k + \sum_{k=0,2,4} M^k m_k + \sum_{k=2,4,6} P^k p_k \quad , \tag{1}$$

where $F^k(nf,nf)$'s and ζ_f represent the radial parts of the electrostatic and spin-orbit interaction, respectively, between f electrons, and f_k and $\alpha_{s.o.}$ are the angular parts of these interactions. The parameters α, β, and γ are associated with the two-body effective operators of the configuration interaction and the T^k's are the corresponding parameters for the three-body-configuration interaction. The M^k parameters arise from spin-spin and spin-other-orbit interactions and the P^k parameters represent the electrostatic-spin-orbit interaction with higher configurations. The T^k, M^k, and P^k are the radial parts of the

interactions, whereas t_k, m_k, and p_k are the corresponding angular parts. For the different interaction mechanisms present the angular parts can be evaluated exactly, while the radial portions are treated as parameters.

For D_{2d} symmetry, the crystal-field Hamiltonian can be expressed in terms of five phenomenological parameters B_q^k and the angular tensor operators C_q^k. For this particular symmetry, the values of |q| are limited to 0 and 4 and the Hamiltonian is given by [1]:

$$H_{CF} = B_0^2C_0^2 + B_0^4C_0^4 + B_4^4\left[C_{-4}^4 + C_4^4\right] + B_0^6C_0^6 + B_4^6\left[C_{-4}^6 + C_4^6\right]. \qquad (2)$$

The quality of the fits to the above expressions was determined from the deviation σ (in cm^{-1}), which is defined as:

$$\sigma = \sum\left[\frac{\left(E_{exp} - E_{calc}\right)^2}{(n-p)}\right]^{\frac{1}{2}}, \qquad (3)$$

where n is equal to the number of levels and p is the number of parameters that are varied freely. For fits to the lanthanide ions' energy-level structure this value is generally on the order of 10 to 15 cm^{-1}. However, for the actinides σ is larger.

Results

1. Ground-State Absorption and Fluorescence Line Narrowing Spectroscopy

Laser-selective excitation was used to observe the GSA transitions to energy levels in the range 16,400 to 26,300 cm^{-1}. These spectra enabled some refinement of the experimental energy levels obtained previously by conventional absorption spectroscopy [5]. The experimentally determined levels appear in the fourth column of Table II.

The lowest energy $^8S_{7/2} \leftrightarrow {}^6D_{7/2}(1)$ transitions have inhomogeneously-broadened FWHM line widths of approximately 2.3 cm^{-1}, as measured from absorption spectra and from fluorescence spectra following broad-band excitation, Figure 1(a). When FLN was used to resolve the transitions to the four crystal-field levels of the nominally $^8S_{7/2}$ ground state, Figure 1(b), the observed line widths were reduced to the FWHM line width of the dye laser of approximately 0.8 cm^{-1}. Numerous satellite transitions also appeared in the FLN spectra as reported previously [5]. They appeared in both excitation and fluorescence, and exhibited common displacements from the principal electronic transitions, which were equal to one of the crystal-field splittings in the $^8S_{7/2}$ ground state.

Fluorescence satellites are shown in Figure 1(b). In this case the pump laser was resonant with a subset of sites within the inhomogeneously broadened $^8S_{7/2}(2) \rightarrow {}^6D_{7/2}(1)$ absorption transition. These subsites produced the principal fluorescence transitions, labeled as '2', in Figure 1(b). However, another subset of sites within the inhomogeneously broadened $^8S_{7/2}(1) \rightarrow {}^6D_{7/2}(1)$ absorption transition were also excited. It was fluorescence from these subsites which produced the satellites labeled as '1'. One of these satellites coincided with one of the principal transitions, producing an apparent enhancement in the intensity of this feature. The satellite labeled as '3' was due to the

excitation of yet another subset of sites in the inhomogeneously broadened $^8S_{7/2}(3) \rightarrow {}^6D_{7/2}(1)$ transition. The satellites labeled as '1' in Figure 1(b) have an average displacement from the respective principal features of 3.42 cm^{-1}. This corresponds to the crystal-field splitting between the $^8S_{7/2}(1)$ and $^8S_{7/2}(2)$ levels, measured as 3.49 cm^{-1}. The satellite labeled as '3' was displaced by 4.65 cm^{-1} from the principal $^6D_{7/2}(1) \rightarrow {}^8S_{7/2}(1)$ transition, which compares to a measured splitting between the $^8S_{7/2}(2)$ and $^8S_{7/2}(3)$ levels of 4.64 cm^{-1}.

Excitation satellites are shown in Figure 1(c). In this case the monochrometer was set so that a subset of sites within the $^6D_{7/2}(1) \rightarrow {}^8S_{7/2}(4)$ fluorescence transition was selected. The excitation features of these subsites are labeled as '4' in the spectrum. The relative intensities of these transitions were modified by the Boltzman population distribution in the four $^8S_{7/2}$ crystal-field states [5]. Fluorescence from another set of subsites within the inhomogeneously broadened $^6D_{7/2}(1) \rightarrow {}^8S_{7/2}(3)$ transition was also detected. Excitation transitions of these subsites are labeled as '3'. As before, a slight enhancement in one of the principal transitions was observed due a coincidence with one of the satellite transitions. The satellites labeled as '3' in Figure 1(c) have an average displacement from the respective principal transitions of 1.40 cm^{-1}. This corresponds to the measured 1.39 cm^{-1} crystal-field splitting between the $^8S_{7/2}(3)$ and $^8S_{7/2}(4)$ levels.

The observation of satellite transitions with common displacements from the principal transitions and accompanied by an enhancement of the principal transition to or from the selected crystal-field component, characterizes this peculiar manifestation of site selectivity through FLN. Monitoring the $^6D_{7/2}(1) \rightarrow {}^8S_{7/2}(1)$ transition minimized the intensity of the satellites observed in excitation and simplified the interpretation of the GSA spectra. This transition is 3.5 cm^{-1} away from its neighboring $^6D_{7/2}(1) \rightarrow {}^8S_{7/2}(2)$ transition, which is comparatively weak.

2. Excited-State Absorption Spectroscopy

Sequential excitation was used to observe ESA transitions to energy levels between 27,700 and 35,700 cm^{-1}. The energy range between 35,700 and 37,600 cm^{-1} was inaccessible in these experiments due to strong GSA to the $^6P_{5/2}$ multiplet. ESA was also observed to levels between 37,600 and 40,600 cm^{-1}, with both GSA and ESA features appearing in these spectra, Figure 2(a). They were distinguishable, as the latter did not appear when the first laser pulse was removed by blocking the beam, Figure 2(b). However, as a result of lifetime broadening arising from the high density of states in this energy range, only a few of the ESA transitions were narrow enough to be distinguished from the underlying GSA signal. Many more transitions are predicted by the crystal-field calculations in this energy range than were observed. Because of the difficulty in assigning these measured levels, they were not used in the fitting procedure.

In Figure 3 an ESA spectrum, showing the transitions to the $^6D_{7/2}{}'$ multiplet, is compared to the corresponding GSA spectrum which was obtained with a Xe lamp. Absorption from at least two of the ground-state levels was observed to each of the $^6D_{7/2}{}'(1)$ and $^6D_{7/2}{}'(2)$ levels. The originating levels for ground-state absorption to the $^6D_{7/2}{}'(4)$ level can not be determined without reference to the ESA spectrum. The $^6D_{7/2}(1) \rightarrow {}^6D_{7/2}{}'(3)$ transition appeared only weakly in the ESA spectrum and apparently has a comparatively small transition moment. This demonstrates how the information obtained by these two spectroscopic techniques is complementary. The other weak and unlabeled transitions in the ESA spectrum were attributed to minor Cm^{3+} centers, reported previously [5].

Figure 4 shows the polarization behavior of the ESA transitions to the $^6G_{3/2}$ and $^6G_{9/2}$ multiplets at 32,000 cm^{-1}. As reported earlier [4,5], single-photon electronic transitions exhibited only weak polarization behavior in this material. The electric-dipole selection rules for D_{2d} point-group symmetry allow only σ-polarized $\Gamma_6 \leftrightarrow \Gamma_6$ and $\Gamma_7 \leftrightarrow \Gamma_7$ transitions. Therefore, approximately half the electronic transitions should disappear in the π-polarized spectra. This was not observed experimentally in $Cm^{3+}/LuPO_4$. Although this weak polarization behavior is not understood, there may be some contribution to the electric-dipole forbidden π-polarized spectra from magnetic dipole transitions as found previously for some electonic transitions in $Cm^{3+}/LaCl_3$ [3].

3. Time Resolved Fluorescence Line Narrowing

Inter-ion energy transfer is demonstrated in the TRFLN spectra of Figure 5. Each of these spectra has been obtained with a different time-gate delay. They have been scaled so that the strongest feature in each spectrum appears with the same height, as the intensity of fluorescence from the $^6D_{7/2}$ multiplet was modulated by its radiative decay with a fluorescence lifetime of 580 μs. The 16530.1 cm^{-1} laser pulse selectively pumped a subset of sites within the inhomogeneously broadened $^8S_{7/2}(1) \rightarrow {}^6D_{7/2}(1)$ excitation transition centered at 16528.2 cm^{-1}. These subsites (line 1) dominated the fluorescence spectrum obtained 0.01 ms after the laser pulse. The excitation energy was subsequently transferred to other Cm^{3+} subsites. In fluorescence this was observed as a redistribution of the fluorescence intensity within the inhomogeneously broadened $^6D_{7/2}(1) \rightarrow {}^8S_{7/2}(1)$ transition. The fluorescence feature associated with these other subsites (line 1') grew and migrated, until it had the same shape as the Lorentzian distribution of subsites within the inhomogeneously-broadened fluorescence transition. This redistribution was also evident

within the inhomogeneously broadened $^6D_{7/2}(1) \rightarrow {}^8S_{7/2}(2)$ fluorescence transition centered at 16524.7 cm^{-1}.

The quantity used to analyze the transfer process is the ratio $R(t)$ of the intensity of the FLN line, $I_1(t)$, to the total intensity of the inhomogeneously-broadened line, $I_1(t)+I_{1'}(t)$ [8]:

$$R(t)=\frac{I_1(t)}{I_1(t)+I_{1'}(t)} . \qquad (4)$$

Sequences of TRFLN spectra were recorded at temperatures of 4, 8 and 12 K. In each case the time-gate delay was varied from 0.01 to 3.6 ms, in increments of 0.6 ms, with the time gate open for 0.1ms. Two particular difficulties arose when analyzing these spectra using a line-fitting procedure. The small 9.5 cm^{-1} crystal-field splitting of the nominally $^8S_{7/2}$ ground state makes it impossible to isolate just one inhomogeneously broadened fluorescence transition. The $^6D_{7/2}(1) \rightarrow {}^8S_{7/2}(1)$ transition was selected for quantitative analysis because it is 3.5 cm^{-1} away from the comparatively weak $^6D_{7/2}(1) \rightarrow {}^8S_{7/2}(2)$ transition. However, as is evident from Figure 5, the contributions from the inhomogeneously broadened $^6D_{7/2}(1) \rightarrow {}^8S_{7/2}(2)$ and $^6D_{7/2}(1) \rightarrow {}^8S_{7/2}(3)$ transitions must also be considered. The second difficulty arises from the fact that the line shape of the evolving 1′ feature was asymmetric. Energy was apparently transferred sequentially across the inhomogeneously broadened line. An approximation is implicit in fitting this line to a Lorentzian function. It must also be remembered that the time gate was open for a finite time of 0.1ms, compared to the delay time increment of 0.6 ms. One effect of this was that some energy transfer is evident in the '0.01 ms' spectrum of Figure 5.

To subtract the constant background signal due to the dark current, a linear baseline of slope zero was also fitted to each spectrum. Initially, the width and positions of lines 1

and 2 were obtained by a fit to the 0.01 ms spectrum. They were then fixed at these values in all subsequent fits. In the first fit to each spectrum, the widths of lines 1′, 2′, and 3′ were fixed at the measured value for the inhomogeneously-broadened line width (2.3 cm^{-1}). The positions of lines 2′ and 3′ were also fixed to the peak energies of the inhomogeneously-broadened transitions at 16524.7 and 16520.1 cm^{-1}. All of the peak heights and the position of line 1′ were varied. In the second fit, the width of line 1′ was also varied. For the final fit, the widths of lines 2′ and 3′ were set to the best fit value for the line width of 1′. R(t) could then be calculated from the best fit values for the widths and peak heights of lines 1 and 1′.

For all the reasons given above these experimental values of R(t) are only approximations of the true values. However, there is surprisingly good agreement between values of R(t) calculated from the $^6D_{7/2}(1) \rightarrow {}^8S_{7/2}(1)$ transition and those calculated from the $^6D_{7/2}(1) \rightarrow {}^8S_{7/2}(2)$ transition, which suggests that the former have been well determined. As is customary, the logarithm of R(t) is plotted in Figure 6, although R(t) is not generally a simple exponential decay function [8]. The nominal 1/*e* decay time of R(t) gives a measure of the energy-transfer rate. The measured decay times were 2.7 ms at 4 K, 1.1 ms at 8 K, and 1.1 ms at 12 K .

TRFLN data can also be used to determine the type of multipole interaction mediating the energy transfer. In a dilute system, the approximate transfer behavior is given by [8]:

$$R(t) \cong -\frac{4\pi N}{3}.r_0^3.(W_0 t)^{3/s}.\Gamma\left(1-\frac{3}{s}\right).F \quad , \qquad (5)$$

where N is the number of optically active ions per unit volume, W_0 is the energy-transfer rate, r_0 is the corresponding nearest-neighbor distance, $\Gamma()$ is the gamma function of the

quantity in brackets, and the value of F depends on the specific transfer model used (F=1 if no back transfer is included). The parameter s is equal to 6, 8, or 10 for dipole-dipole, dipole-quadruple, and quadruple-quadruple interactions respectively. It can be derived from the experimental values for R(t) by plotting $\ln[R^{-1}(t)]$ *vs* $\ln[t]$, as in Figure 7. A straight-line least-squares fit to this 4 K data gives a slope (3/s) of 0.51, corresponding to a value of 5.9 for s.

Discussion

The experimental energy levels were fitted to the parameters of a phenomenological Hamiltonian, as described above. In an earlier study [5] 60 experimental levels were included in the final fit, which had a standard deviation of 30.8 cm^{-1}. LSE spectroscopy confirmed that all but two of these belong to the intrinsic Cm^{3+} center, and 22 additional experimental levels were measured. The calculated levels from the earlier fit were used to assign these new experimental levels. Starting from the earlier best-fit parameters [5, 12], a new fit was obtained using all 80 levels with a deviation σ of 28.4 cm^{-1}. The final parameters are listed in Table III. The calculated and experimental energy levels are compared in Table II. The quality of this fit is better than that obtained previously, but the values of the parameters are only slightly different. Thus the discussion and conclusions derived from the previous analysis [5] still hold.

Subsites of the intrinsic Cm^{3+} center arise from the presence of defects and impurities in the $LuPO_4$ crystal. The electronic transitions were inhomogeneously broadened because the Cm^{3+} ions in different subsites experienced slightly different crystal fields. FLN spectra showed that the crystal-field splittings of the nominally $^8S_{7/2}$ multiplet differed by less than 0.1 cm^{-1} between subsites within these inhomogeneously-broadened

transitions. The observed broadening was mostly due to changes in the crystal-field splittings of the excited multiplets. This result is expected, as the overall crystal-field splitting of the nominally $^8S_{7/2}$ multiplet is just 9.5 cm^{-1}, which is much smaller the splittings determined for the higher energy multiplets. For example, the $^6D_{7/2}$ multiplet had an overall splitting of 440 cm^{-1}.

After the Cm^{3+} ions were excited with a narrow bandwidth laser, the energy was transferred from the directly excited subsites within the FLN line to the other subsites of the intrinsic Cm^{3+} center. This was observed as a migration of fluorescence intensity across the inhomogeneously-broadened transition. Such sequential transfer minimizes the energy mismatch in each energy-transfer step and satisfies energy conservation. Higher energy transfer rates were observed when the sample temperature was increased. This is characteristic of phonon-assisted energy transfer, which has been observed before in lanthanide doped materials. Measured phonon line widths in $LuPO_4$ range from 1 to 10 cm^{-1} [13]. The measured energy-transfer rates at 8 K and 12 K were equal, which is a surprising result. However, since the sample temperature was measured indirectly, it is possible that differences in the actual sample temperature were not as large as the temperature sensor indicated. The TRFLN results obtained at 4 K indicate that dipole-dipole interactions are responsible for the observed energy transfer.

Conclusions

Laser selective excitation techniques have been used to measure 80 crystal-field levels for the Cm^{3+} ion located at the intinsic D_{2d} symmetry site of $LuPO_4$. Inhomogeneous broadening of the electronic transitions, which is attibuted to lattice defects and impurities, could be resolved by fluorescence line narrowing. This broadening is

responsible for the satellite features reported previously for transitions between the nominally $^8S_{7/2}$ ground multiplet and other excited multiplets. Excited-state absorption was also used to obtain site selective excitation spectra of levels up to 35,700 cm^{-1}. These experimental levels have been fitted using a least-squares fitting procedure.

Energy transfer between the different subsites of the intrinsic Cm^{3+} center was observed by time resolved fluorescence line narrowing. Sequences of TRFLN spectra were recorded and used to establish that electric-dipole interactions mediate this energy transfer. The transfer rate increased on warming the crystal above 4 K. This increase is indicative of phonon-assisted energy-transfer processes. This is believed to be the first report of inter-ion energy transfer in a Cm^{3+} doped system.

Acknowledgement

This research was sponsored by the Director, Office of Energy Research, Office of Basic Energy Sciences, Chemical Sciences Division of the U.S. Department of Energy under Contract No. De-AC03-76SF00098 with the University of California and by the Division of Material Sciences, U.S. Department of Energy under Contract No. DE-AC05-84OR21400 with Martin Marietta Energy Systems, Inc. The authors are indebted for the use of the ^{248}Cm to the Division of Chemical Sciences, Office of Basic Energy Sciences, through the transplutionium element production facilities at Oak Ridge National Laboratory. The authors also acknowledge with thanks the excellent technical contributions of H. E. Harmon and C. B. Finch.

References

1. B. G. Wybourne, "Spectroscopic Properties of Rare Earths", Interscience, New York, 1965.

2. A. Abragam and B. Bleaney, "Electron Paramagnetic Resonance of Transition Ions", Oxford, London, 1970.

3. G. K. Lui, J. V. Beitz, and J. Huang, *J. Chem. Phys.* **99**, 3304 (1993).

4. W. K. Kot, N. M. Edelstein, M. M. Abraham, and L. A. Boatner, *Phys. Rev. B* **48**, 12704 (1993).

5. J. Sytsma, K. M. Murdoch, N. M. Edelstein, L. A. Boatner, and M. M. Abraham, *Phys. Rev. B* **52**, 12668 (1995).

6. K. M. Murdoch, A.-D. Nguyen, N. M. Edelstein, J.-C. Gâcon, and S. Hubert, unpublished.

7. N. A. Stump, G. M. Murray, G. D. Del Cul, R. G. Haire, and J. R. Peterson, *Radiochimica Acta* **61**, 129 (1993).

8. W. M. Yen, "Spectroscopy of Solids Containing Rare-Earths", in *Modern Problems in Condensed Matter Sciences* (North Holland) **21**, 185 (1987).

9. L. A. Boatner, G. W. Beall, M. M. Abraham, C. B. Finch, R. J. Floran, P. G. Huray, and M. Rappaz, *"Management of Alpha-Contaminated Wastes"*, p. 114, IAEA-SM-245/73, International Atomic Energy Agency, Vienna (1981).

10. M. Rappaz, L. A. Boatner, and M. M. Abraham, *J. Chem. Phys.* **73**, 1045 (1980).

11. W. T. Carnall, H. Crosswhite, H. M. Crosswhite, J. P. Hessler, N. M. Edelstein, J. G. Conway, G. V. Shalimoff, and R. Sarup, *J. Chem. Phys.* **72**, 5089 (1980).

12. In Table I of reference 5, the headings for the second and third columns were inadvertently transposed.

13. A.-D. Nguyen, "Polarization Dependance of Two-Photon Transition Intensities in Rare-Earth Doped Crystals", Ph.D. Thesis, University of California at Berkeley (1996).

Table I. The laser dyes used in the tunable PDL-3 dye laser to measure the Cm^{3+} energy levels.

Laser Dye	GSA Range (cm^{-1})	ESA Range (cm^{-1})
LDS 867		27700 - 28200
LDS 765		29200 - 29700
LDS 751		29500 - 30300
LDS 750		30100 - 30700
LDS 698		30500 - 31500
DCM		31500 - 32500
Rhodamine 640	16400 - 17200	
Rhodamine 610		33200 - 33800
Rhodamine 590		33800 - 34500
Rhodamine 575		34100 - 32900
Coumarin 500	18500 - 20600	35000 - 35700
Coumarin 460	21100 - 22200	37600 - 38700
Coumarin 440	22000 - 23000	38500 - 39500
Stilbene 420	22500 - 24100	39000 - 40600
LD 390 + S 420	24300 - 26300	

Table II. Calculated and experimental energy levels for Cm^{3+} diluted in $LuPO_4$. The $^8S_{7/2}$ multiplet levels have an experimental uncertainty of ± 0.02 cm^{-1}. All the other experimental levels have an uncertainty of ± 1.0 cm^{-1}.

Crystal-Field Level	Largest $^{2S+1}L_J$ Comp.	Calculated Energy (cm^{-1})	Experimetal Energy (cm^{-1})	Difference ($E_{exp.}$-$E_{calc.}$) (cm^{-1})
$1\Gamma_7$	$^8S_{7/2}$	-8.2	0.00	8.2
$1\Gamma_6$	$^8S_{7/2}$	-4.1	3.49	7.6
$2\Gamma_7$	$^8S_{7/2}$	7.8	9.52	1.7
$2\Gamma_6$	$^8S_{7/2}$	8.7	8.13	-0.6
$3\Gamma_7$	$^6D_{7/2}$	16532.9	16528	-4.9
$3\Gamma_6$	$^6D_{7/2}$	16556.8	16577	20.2
$4\Gamma_7$	$^6D_{7/2}$	16959.1	16945	-14.1
$4\Gamma_6$	$^6D_{7/2}$	17152.1	17122	-30.1
$5\Gamma_6$	$^6P_{5/2}$	19835.7	19778	-57.7
$5\Gamma_7$	$^6P_{5/2}$	19992.6	20017	24.4
$6\Gamma_6$	$^6P_{5/2}$	20109.5	20181	71.5
$7\Gamma_6$	$^6I_{7/2}$	21477.7	21446	-31.7
$6\Gamma_7$	$^6I_{7/2}$	21480.6	21472	-8.6
$8\Gamma_6$	$^6I_{7/2}$	21640.4	21614	-26.4
$7\Gamma_7$	$^6I_{7/2}$	21748.5	21726	-22.5
$8\Gamma_7$	$^6P_{3/2}$	22047.1	22044	-3.1
$9\Gamma_6$	$^6P_{3/2}$	22176.4	22142	-34.4
$9\Gamma_7$	$^6I_{9/2}$	22529.3	22585	55.7
$10\Gamma_6$	$^6I_{9/2}$	22685.1	22666	-19.1

$10\Gamma_7$	$^6I_{9/2}$	22706.0		
$11\Gamma_7$	$^6I_{9/2}$	22969.3	22941	-28.3
$11\Gamma_6$	$^6I_{9/2}$	22997.2	23028	30.9
$12\Gamma_7$	$^6I_{11/2}$	24582.7	24612	29.3
$13\Gamma_7$	$^6I_{17/2}$	24685.7	24682	-3.7
$12\Gamma_6$	$^6I_{17/2}$	24690.2	24695	4.8
$14\Gamma_7$	$^6I_{17/2}$	24724.0	24728	4
$13\Gamma_6$	$^6I_{17/2}$	24747.4		
$15\Gamma_7$	$^6I_{17/2}$	24774.6	24794	19.4
$14\Gamma_6$	$^6I_{17/2}$	24832.8	24839	6.2
$16\Gamma_7$	$^6I_{17/2}$	24861.5	24869	7.5
$15\Gamma_6$	$^6I_{17/2}$	24864.1		
$17\Gamma_7$	$^6I_{17/2}$	24896.0	24885	-11
$16\Gamma_6$	$^6I_{11/2}$	24927.8	24923	-4.8
$18\Gamma_7$	$^6I_{11/2}$	24942.6	24942	-0.6
$17\Gamma_6$	$^6I_{11/2}$	24967.0	24978	11
$19\Gamma_7$	$^6I_{11/2}$	25102.8	25100	-2.8
$18\Gamma_6$	$^6I_{11/2}$	25181.2	25178	-3.3
$19\Gamma_6$	$^6D_{9/2}$	25424.3	25444	19.7
$20\Gamma_7$	$^6D_{9/2}$	25559.2		
$21\Gamma_7$	$^6I_{13/2}$	25682.0	25651	-31
$20\Gamma_6$	$^6I_{13/2}$	25690.0	25698	8
$21\Gamma_6$	$^6I_{13/2}$	25761.1	25723	-38.1
$22\Gamma_6$	$^6I_{13/2}$	25826.5		
$22\Gamma_7$	$^6I_{13/2}$	25829.1	25799	-30.1
$23\Gamma_7$	$^6D_{9/2}$	25860.0	25859	-1
$23\Gamma_6$	$^6I_{13/2}$	25902.2		

$24\Gamma_7$	$^6I_{13/2}$	25958.8	25958	-0.8
$24\Gamma_6$	$^6I_{13/2}$	26014.3	25998	-16.3
$25\Gamma_7$	$^6I_{15/2}$	26099.2	26085	-14.2
$25\Gamma_6$	$^6I_{15/2}$	26113.3		
$26\Gamma_7$	$^6D_{9/2}$	26121.9		
$26\Gamma_6$	$^6I_{15/2}$	26222.8	26212	-10.8
$27\Gamma_7$	$^6I_{15/2}$	26238.0		
$27\Gamma_6$	$^6I_{15/2}$	26263.4	26263	-0.4
$28\Gamma_7$	$^6I_{15/2}$	26319.4	26326	6.6
$28\Gamma_6$	$^6I_{15/2}$	26375.0		
$29\Gamma_7$	$^6I_{15/2}$	26411.5	26491	79.5
$29\Gamma_6$	$^6D_{7/2}$	27872.3	27875	2.7
$30\Gamma_7$	$^6D_{7/2}$	27916.4	27899	-17.4
$30\Gamma_6$	$^6D_{7/2}$	27975.9	27998	22.1
$31\Gamma_7$	$^6D_{7/2}$	28022.8	28022	-0.8
$31\Gamma_6$	$^6G_{5/2}$	29290.3	29302	11.7
$32\Gamma_7$	$^6G_{5/2}$	29428.1	29432	3.9
$32\Gamma_6$	$^6G_{5/2}$	29459.5	29473	13.5
$33\Gamma_7$	$^6D_{1/2}$	29591.4	29565	-26.4
$33\Gamma_6$	$^6I_{7/2}$	29831.8		
$34\Gamma_7$	$^6I_{7/2}$	29889.1	29908	18.9
$35\Gamma_7$	$^6I_{7/2}$	29980.1	29990	9.9
$34\Gamma_6$	$^6I_{7/2}$	30071.2		
$35\Gamma_6$	$^6D_{5/2}$	30223.2		
$36\Gamma_6$	$^6D_{5/2}$	30260.3		
$36\Gamma_7$	$^6D_{5/2}$	30329.4	30330	0.6
$37\Gamma_7$	$^6D_{3/2}$	30396.7	30391	-5.7

$37\Gamma_6$	$^6D_{3/2}$	30513.9		
$38\Gamma_6$	$^6G_{11/2}$	30657.4	30678	20.6
$38\Gamma_7$	$^6G_{11/2}$	30742.3	30707	-35.3
$39\Gamma_7$	$^6G_{11/2}$	30857.7	30826	-31.7
$39\Gamma_6$	$^6G_{11/2}$	30887.3	30858	-29.3
$40\Gamma_7$	$^6G_{11/2}$	31050.3	31067	16.7
$40\Gamma_6$	$^6G_{11/2}$	31162.8		
$41\Gamma_7$	$^6G_{9/2}$	31708.7	31703	-5.7
$42\Gamma_7$	$^6G_{9/2}$	31753.4	31758	4.6
$41\Gamma_6$	$^6G_{9/2}$	31809.1		
$43\Gamma_7$	$^6G_{9/2}$	31811.1	31834	22.9
$42\Gamma_6$	$^6G_{9/2}$	31893.2	31943	49.8
$43\Gamma_6$	$^6G_{3/2}$	32036.7		
$44\Gamma_7$	$^6G_{3/2}$	32155.8	32223	67.2
$44\Gamma_6$	$^6G_{13/2}$	33610.6	33593	-17.6
$45\Gamma_7$	$^6G_{13/2}$	33655.7	33646	-9.8
$45\Gamma_6$	$^6G_{13/2}$	33731.3		
$46\Gamma_6$	$^6G_{13/2}$	33852.7	33818	-34.7
$46\Gamma_7$	$^6G_{13/2}$	33852.7	33863	10.3
$47\Gamma_7$	$^6G_{13/2}$	34033.0	34011	-22
$47\Gamma_6$	$^6G_{13/2}$	34064.0		
$48\Gamma_6$	$^4N_{17/2}$	34436.9		
$48\Gamma_7$	$^4N_{17/2}$	34480.6		
$49\Gamma_7$	$^4N_{17/2}$	34533.0	34542	9
$49\Gamma_6$	$^4N_{17/2}$	34630.7	34653	22.3
$50\Gamma_7$	$^4N_{17/2}$	34662.4	34701	38.6
$50\Gamma_6$	$^4N_{17/2}$	34774.5	34738	-36.5

$51\Gamma_6$	$^4N_{17/2}$	34836.3	34792	-44.3
$51\Gamma_7$	$^4N_{17/2}$	34847.7		
$52\Gamma_7$	$^4N_{17/2}$	34930.0		
$53\Gamma_7$	$^6G_{7/2}$	35013.7		
$52\Gamma_6$	$^4G6_{11/2}$	35098.8	35105	6.2
$54\Gamma_7$	$^4G6_{11/2}$	35141.6		
$55\Gamma_7$	$^6G_{7/2}$	35203.7		
$53\Gamma_6$	$^6G_{7/2}$	35219.1		

Table III. Fitted parameter values for Cm^{3+} diluted in $LuPO_4$. Those values in square brackets were fixed during the fitting procedure. A total of 80 levels were fitted with σ = 28.4 cm^{-1}.

Parameter	Value (cm^{-1})	Error (cm^{-1})
F^2	54066	102
F^4	43487	128
F^6	33078	126
ζ	2869	13
α	27.1	5.3
β	-1270	54
γ	1328	65
T^2	259	52
T^3	[50.0]	
T^4	[40.0]	
T^6	[-360.0]	
T^7	[390.0]	
T^8	[340.0]	
M^0	[1.090]	
M^2	[0.610]	
M^4	[0.414]	
P^2	[912]	
P^4	[507]	
P^6	[338]	
B_0^2	503	41

B_0^4	197	55
B_4^4	-1994	45
B_0^6	-3007	58
B_4^6	626	55

Figure Captions

Figure 1. (a) A fluorescence spectrum obtained by broad-band excitation using a 75W Xe-lamp filtered by a 400 - 5 nm line filter. The four $^6D_{7/2}(1) \rightarrow {}^8S_{7/2}$ transitions are fitted to Lorentzian functions with line widths of 2.3 cm^{-1}. (b) A fluorescence spectrum obtained by selective excitation of subsites in the $^8S_{7/2}(2) \leftrightarrow {}^6D_{7/2}(1)$ transition '*', with monochrometer slits of 35 μm and a time gate open from 2 to 142 μs after each laser pulse. The numbers '*n*' indicate the originating levels $^8S_{7/2}(n)$ of the inhomogeneously broadened excitation transitions resonant with the pump laser. (c) An excitation spectrum obtained by selecting a subset of sites in the $^6D_{7/2}(1) \leftrightarrow {}^8S_{7/2}(4)$ transition '*', with monochrometer slits of 40 μm and a time gate open from 2 to 142 μs after each laser pulse. The numbers '*n*' indicate the terminating levels $^8S_{7/2}(n)$ of the inhomogeneously broadened fluorescence transitions seen by the monochrometer.

Figure 2. (a) A dual laser spectrum showing the $^8S_{7/2} \rightarrow {}^6I_{9/2}$ GSA transitions and some ESA transitions to levels between 39,600 and 40,600 cm^{-1}. In (b) the first laser beam was blocked so that only the GSA transitions appear.

Figure 3. Ground-state and excited-state absorption spectra of transitions to the four levels of the $^6D_{7/2}{}'$ multiplet. The GSA spectrum was obtained using a Xe lamp as the light source. The ESA spectrum was obtained using two-dye lasers as excitation sources and is site selective.

Figure 4. π (solid line) and σ (dashed line) polarized excited-state absorption spectra of transitions to the $^6G_{3/2}$ and $^6G_{9/2}$ multiplets.

Figure 5. Time resolved fluorescence line narrowing spectra showing energy transfer between the intrinsic Cm^{3+} ions at a temperature of 12 K. The laser selectively pumped a subset of sites within the $^8S_{7/2}(1) \rightarrow {}^6D_{7/2}(1)$ transition. These spectra were recorded with the time gate opened at 0.01, 0.6, 1.2, and 1.8 ms, respectively, after the laser pulse. The width of the time gate was 0.1 ms and the monochrometer slits were 28 μm. The numbers '*n*' indicate the terminating levels $^8S_{7/2}(n)$ of the $^6D_{7/2} \rightarrow {}^8S_{7/2}$ fluorescence transitions. Lorentzian functions have been fitted to the features in these spectra.

Figure 6. Plots of ln[R(t)] *vs* t using the best fit intensities for the $^8S_{7/2}(1) \rightarrow {}^6D_{7/2}(1)$ transition obtained from the time resolved fluorescence line narrowing experiments. This data was recorded at temperatures of 4 K (•), 8 K (x), and 12 K (+). A least-squares fit to a straight-line function gives decay times of 2.7 ms at 4 K, 1.1 ms at 8 K, and 1.1 ms at 12 K

Figure 7. A plot of $\ln[R^{-1}(t)]$ *vs* Ln[t] for the $^8S_{7/2}(1) \rightarrow {}^6D_{7/2}(1)$ transition, from the time resolved fluorescence line narrowing experiments at 4 K. A least-squares fit to a straight-line function gives a slope of 0.51.

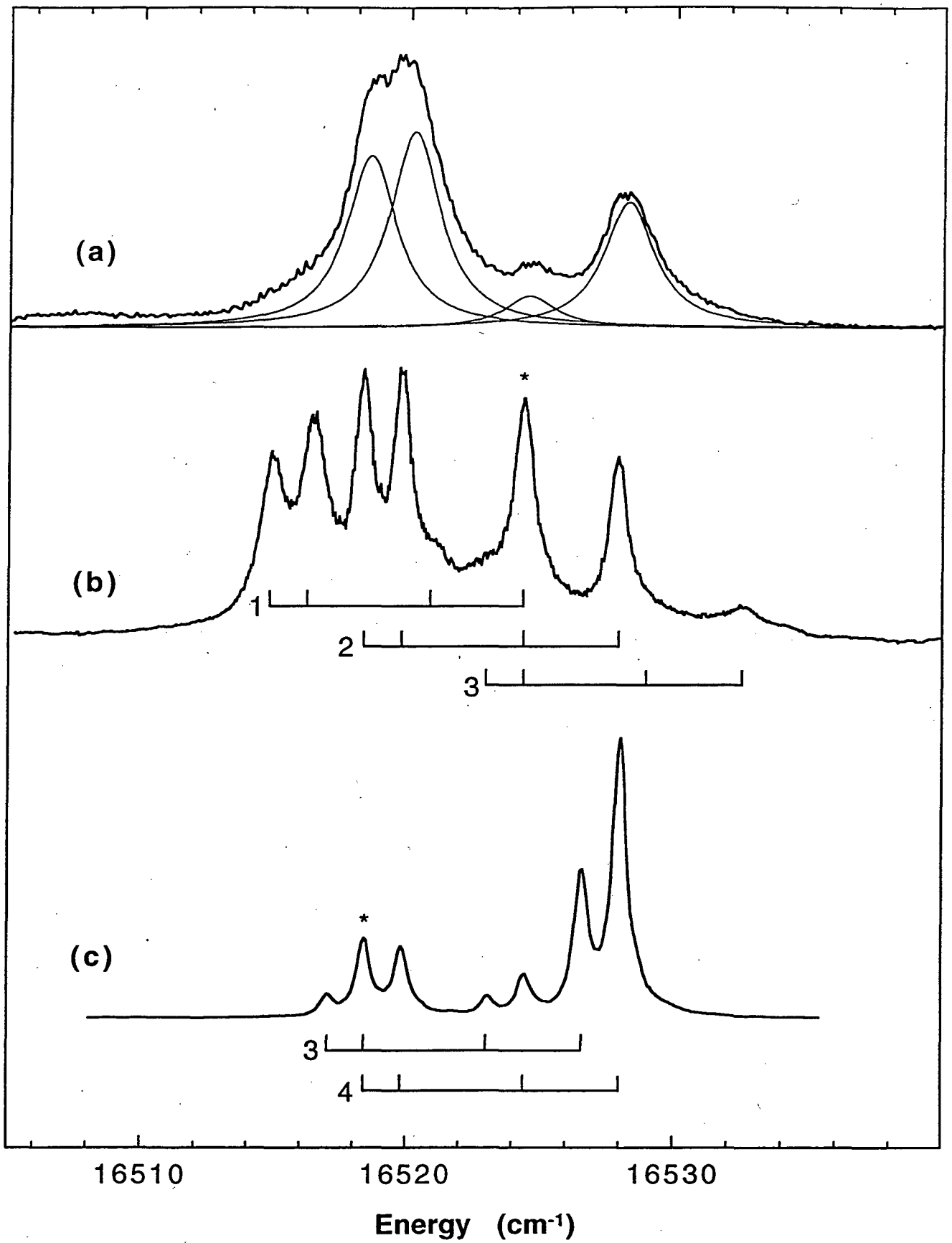
(a)
(b)
*
1
2
3
(c)
*
3
4
16510
16520
16530
Energy (cm-1)

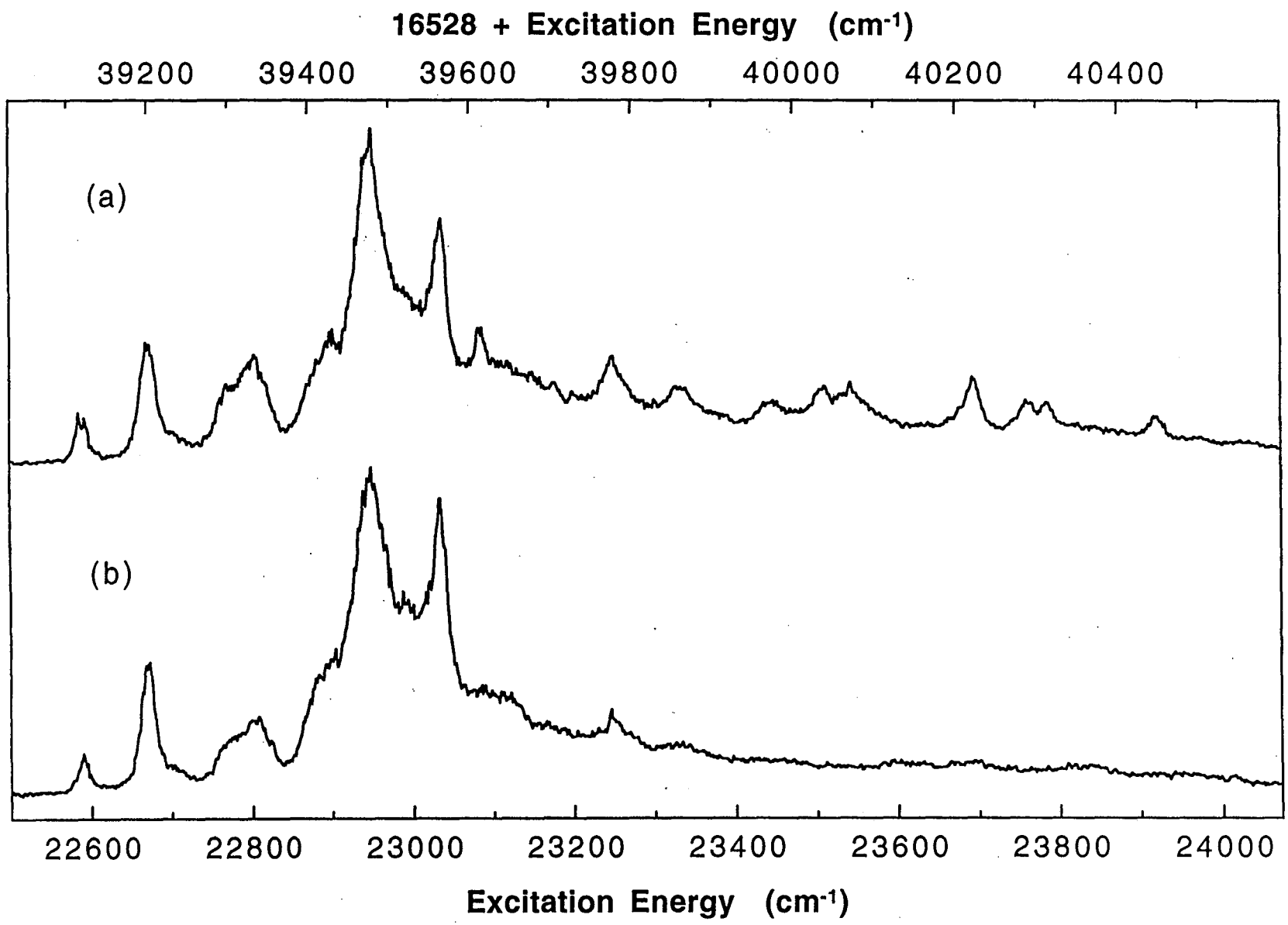
16528 + Excitation Energy (cm-1)
39200
39400
39600
39800
40000
40200
40400
(a)
(b)
22600
22800
23000
23200
23400
23600
23800
24000
Excitation Energy (cm-1)

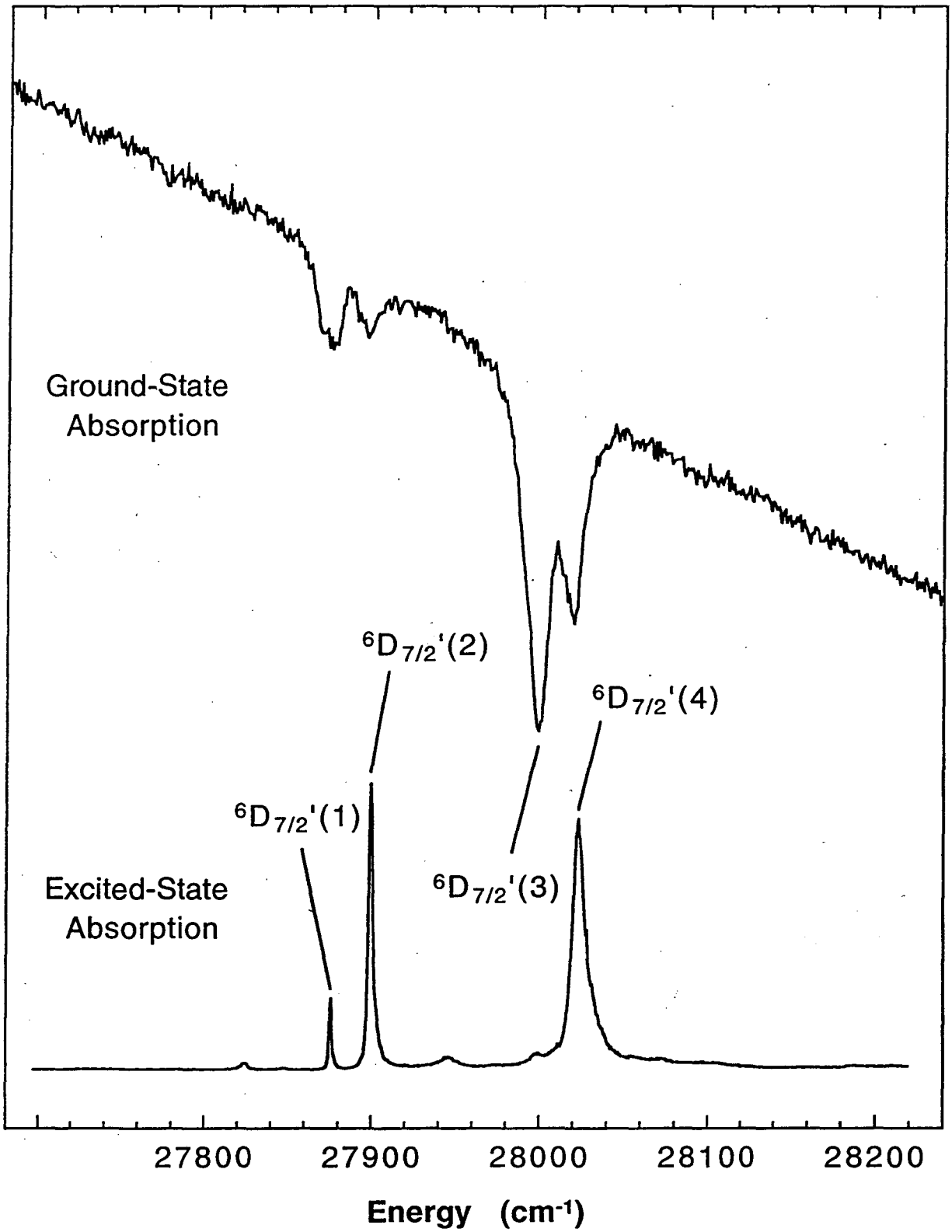
Ground-State
Absorption
$^6D_{7/2}'(2)$
$^6D_{7/2}'(4)$
$^6D_{7/2}'(1)$
$^6D_{7/2}'(3)$
Excited-State
Absorption
27800
27900
28000
28100
28200
Energy (cm^{-1})

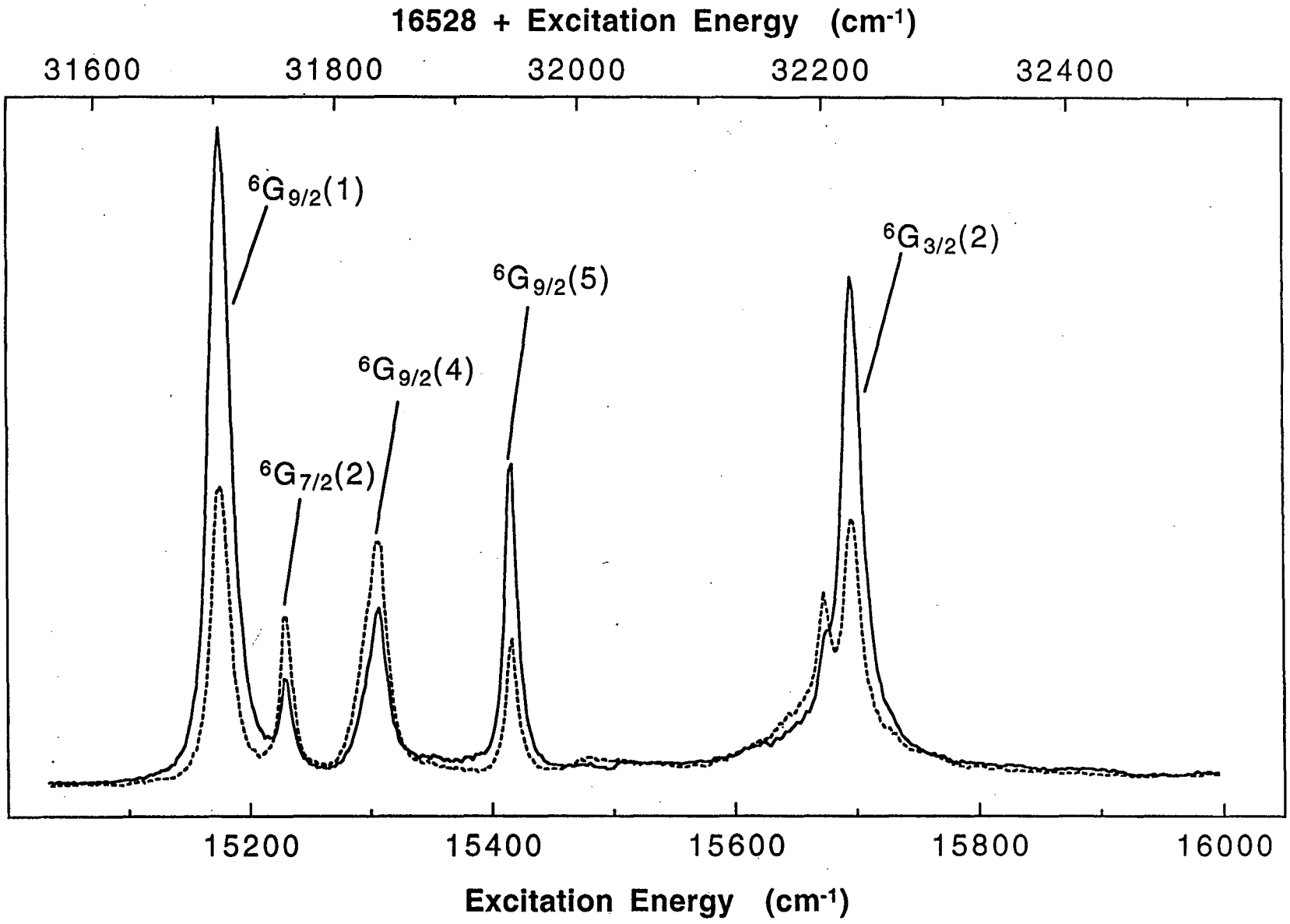
16528 + Excitation Energy (cm-1)
31600
31800
32000
32200
32400
6G9/2(1)
6G7/2(2)
6G9/2(4)
6G9/2(5)
6G3/2(2)
15200
15400
15600
15800
16000
Excitation Energy (cm-1)

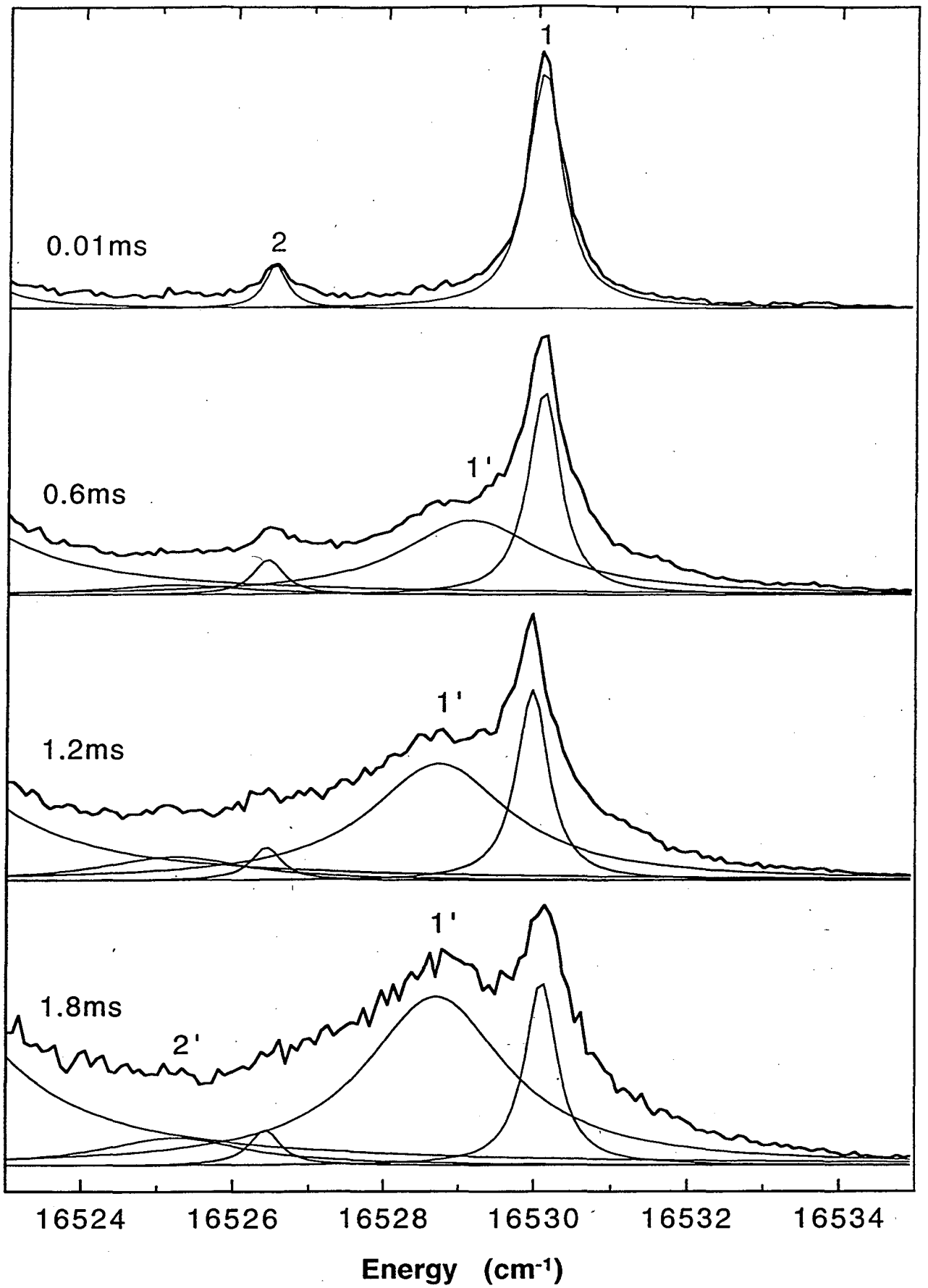
1
0.01ms
2
1'
0.6ms
1'
1.2ms
1'
1.8ms
2'
16524
16526
16528
16530
16532
16534
Energy (cm-1)

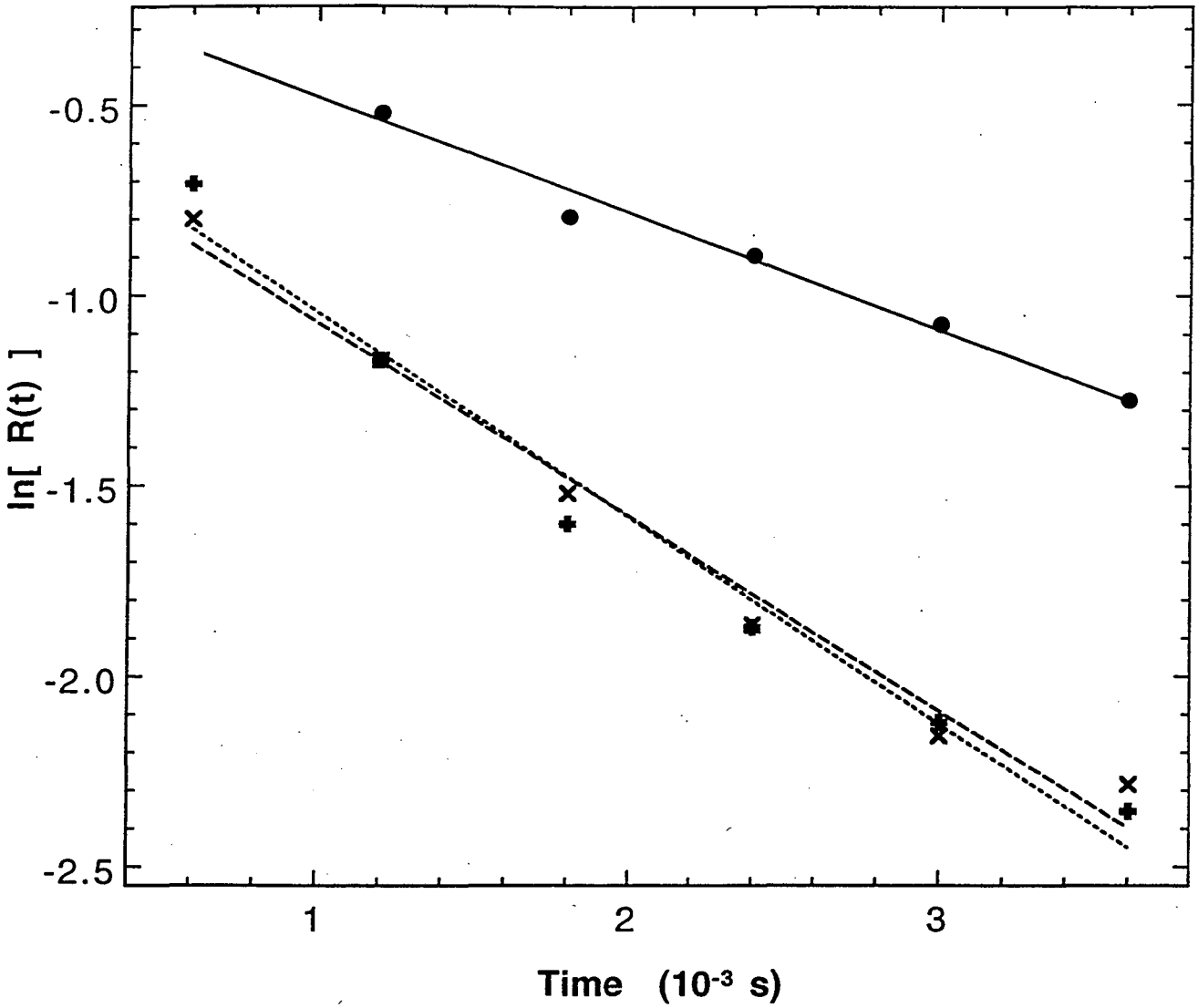
-0.5
-1.0
-1.5
-2.0
-2.5
ln[R(t)]
1
2
3
Time (10-3 s)

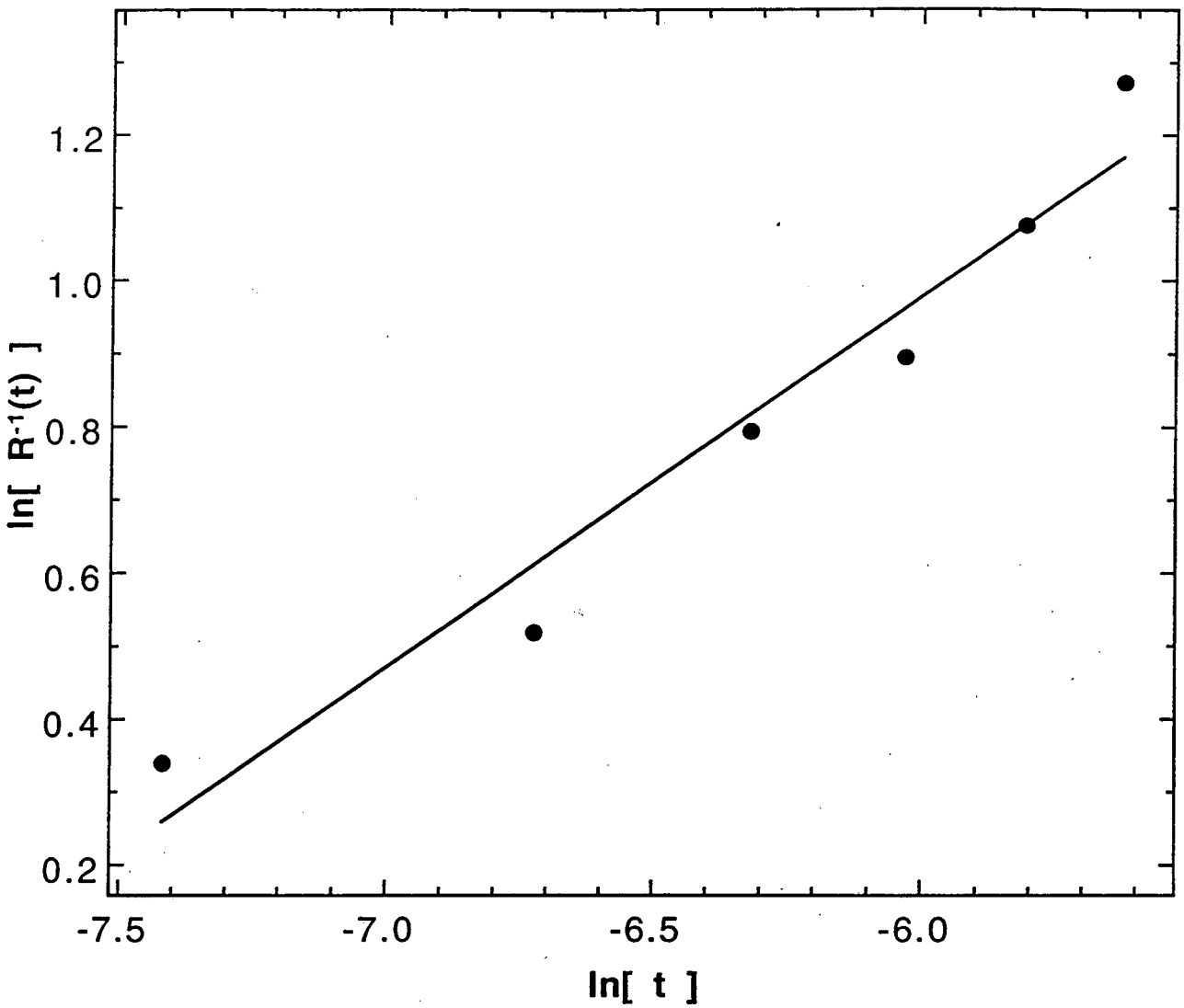
1.2
1.0
0.8
0.6
0.4
0.2
ln[R-1(t)]
-7.5
-7.0
-6.5
-6.0
ln[t]

LAWRENCE BERKELEY NATIONAL LABORATORY
UNIVERSITY OF CALIFORNIA
TECHNICAL & ELECTRONIC INFORMATION DEPARTMENT
BERKELEY, CALIFORNIA 94720